Flux calculation using CARIBIC DOAS aircraft measurements: SO_2 emission of Norilsk

D. Walter,[1,2] K.-P. Heue,[1] A. Rauthe-Schöch,[1] C. A. M. Brenninkmeijer,[1] L. N. Lamsal,[3,4] N. A. Krotkov,[3] and U. Platt[2]

Received 15 December 2011; revised 14 March 2012; accepted 20 April 2012; published 8 June 2012.

[1] Based on a case-study of the nickel smelter in Norilsk (Siberia), the retrieval of trace gas fluxes using airborne remote sensing is discussed. A DOAS system onboard an Airbus 340 detected large amounts of SO_2 and NO_2 near Norilsk during a regular passenger flight within the CARIBIC project. The remote sensing data were combined with ECMWF wind data to estimate the SO_2 output of the Norilsk industrial complex to be around 1 Mt per year, which is in agreement with independent estimates. This value is compared to results using data from satellite remote sensing (GOME, OMI). The validity of the assumptions underlying our estimate is discussed, including the adaptation of this method to other gases and sources like the NO_2 emissions of large industries or cities.

Citation: Walter, D., K.-P. Heue, A. Rauthe-Schöch, C. A. M. Brenninkmeijer, L. N. Lamsal, N. A. Krotkov, and U. Platt (2012), Flux calculation using CARIBIC DOAS aircraft measurements: SO_2 emission of Norilsk, *J. Geophys. Res.*, *117*, D11305, doi:10.1029/2011JD017335.

1. Introduction

[2] SO_2 is an atmospheric trace gas with natural and anthropogenic sources: The major natural direct source is volcanic emissions and therefore strongly varies in space and time. Nevertheless, anthropogenic emissions due to industrial activities are much higher. Apart from uncertainties in estimating sources of SO_2, there are uncertainties due to transport processes, chemical reactions and complex indirect sources like COS and DMS. Sulphur emission leads to the formation of sulphuric acid and ultimately sulphate aerosol. Sulphate particles act as cloud condensation nuclei, increasing the cloud albedo and therefore have a cooling effect on the planet. Moreover there is the direct scattering of sunlight by sulphate aerosol [*Crutzen*, 2006]. Sulphuric acid is the main component of acid rain which has several adverse environmental impacts (e.g., aquatic acidification). A quick impression of the atmospheric SO_2 budget may be gleaned from a statement by *Chin and Jacob* [1996, p. 18,691]: "On a global scale, it is estimated that anthropogenic, biogenic, and volcanic emissions account for 70%, 23%, and 7%, respectively, of the global sulfur source, but that they account for 37%, 42%, and 18%, respectively, of the global column of atmospheric SO_4^{2-}".

[3] Although most of the anthropogenic emissions are related to fossil fuel burning, according to version v4.1 of the EDGAR database (edgar.jrc.ec.europa.eu/, 2011-09-02), the production of metals contributed roughly 10% to the global anthropogenic SO_2 emissions of about 120 Mt in 2005. As sulphur is present in metal ores, SO_2 is emitted during the roasting and refining process [*Environment Australia*, 1999].

[4] One of the biggest copper, nickel and palladium mining and smelting companies worldwide, having facilities in Russia, Australia, Botswana, Finland and South Africa is the Mining and Metallurgical Company "MMC Norilsk Nickel" (http://www.nornik.ru/). A copper plant and a nickel plant are located on the Taimyr Peninsula (Siberia, Russia, 88.2°E, 69.3°N), near the city of Norilsk. Norilsk Nickel is the principal employer in that area, but it is also the reason for Norilsk being one of the most polluted cities in the world [*Blacksmith Institute*, 2007].

[5] In this paper we will make a contribution to better estimating the source strength of SO_2 from metal production by addressing the emissions from this major point source. Our approach falls in the category of studies like *White et al.* [1976] and *Trainer et al.* [1995] who described the flux estimation of urban plumes by airborne in situ measurements. A similar approach, namely the approximation of the source strength by calculating the flux through a certain surface, has been used in other studies, with the difference that remote sensing – ground based [e.g., *Galle et al.*, 2010] as well as airborne [*Melamed et al.*, 2003; *Wang et al.*, 2006] – was used.

[6] The measurements we use are based on Differential Optical Absorption Spectroscopy (DOAS). Unusual is that we use a DOAS system on board of a large passenger aircraft operated in the framework of CARIBIC which happened to pass over Norilsk in October 2010. Thus our paper also communicates the usefulness of such a system

[1]Max Planck Institute for Chemistry, Mainz, Germany.
[2]Institute of Environmental Physics, University of Heidelberg, Heidelberg, Germany.
[3]Atmospheric Chemistry and Dynamics Laboratory, Earth Sciences Division, NASA Goddard Space Flight Center, Greenbelt, Maryland, USA.
[4]University Space Research Association, Columbia, Maryland, USA.

Corresponding author: D. Walter, Max Planck Institute for Chemistry, Hahn-Meitner-Weg 1, DE-55128 Mainz, Germany (david.walter@mpic.de)

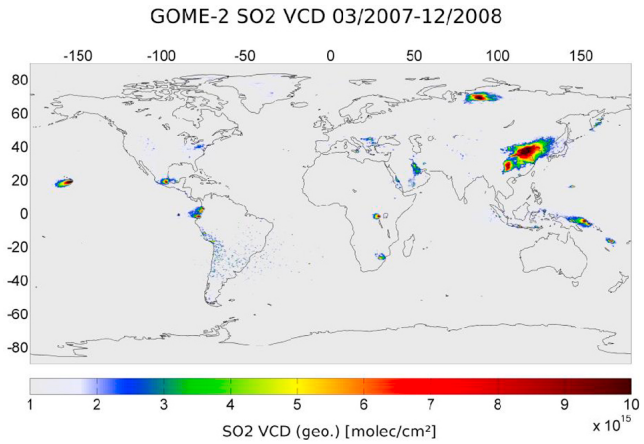

Figure 1. GOME-2 SO_2 measurement (average over the time from March 2007 to December 2008): The strong SO_2 peak in Siberia is caused by Norilsk Nickel. From Christoph Hörmann (Satellite Group of the Max Planck Institute for Chemistry).

for assessing point sources. We show this by means of flux calculations based on the DOAS measurements and wind field data.

[7] Sulphur dioxide is routinely observed by UV-spectroscopy using satellite instruments like GOME, OMI or SCIAMACHY, and an example for Norilsk SO_2 is shown in Figure 1. Therefore, as a third point, we compare our results for Norilsk with those from satellite observations.

[8] Finally, because the CARIBIC instrument is the only remote sensing instrument for measuring trace gases onboard a passenger aircraft, we will briefly discuss how DOAS instruments aboard further passenger aircraft could provide insight into emissions from certain point sources in an economical way.

2. Instrumentation and Data Analysis

2.1. CARIBIC Project

[9] "Civil Aircraft for the Regular Investigation of the atmosphere Based on an Instrument Container" (CARIBIC, http://www.caribic-atmospheric.com/) is a long-term airborne observation system for investigating the atmosphere during regular passenger flights. The aim of CARIBIC is to provide detailed data for a better understanding of atmospheric processes, like long range transport of pollution or stratosphere-troposphere exchange [*Brenninkmeijer et al.*, 2007].

[10] CARIBIC uses a 1.6 ton automated measurement container that is installed in the forward cargo compartment of a Lufthansa Airbus A340-600 once per month. The container is then in use during four consecutive flights. It contains several in-situ instruments (aerosols, humidity and trace gases like CO, CO_2, CH_4, O_3, NO_y). Additionally, air samples and aerosol samples are taken for retrospective laboratory analysis [e.g., *Martinsson et al.*, 2009]. The DOAS instrument constitutes a third category, namely remote sensing. After the flights, the container is deinstalled and the data and samples analyzed.

[11] The container is connected to an inlet system (also denoted as CARIBIC pylon), which is installed permanently under the aircraft's belly. This pylon houses, besides three inlet probes for water, aerosols and trace gases, the three telescopes of the DOAS system.

2.2. DOAS Instrument on CARIBIC

[12] The DOAS instrument on CARIBIC consists of 3 spectrometers which are connected to the inlet pylon via three quartz fibre bundles. In the inlet pylon, three small telescopes with an aperture angle of 1.9° observe scattered sunlight to the right under three elevation angles (see Figure 2). The fibre for the +10° (relative to the horizon) upward looking telescope was broken in 2010, so only the −10° direction and the −82° direction (named "nadir") were available. A detailed description of the instrumentation is given in *Dix* [2007], *Dix et al.* [2009] and *Heue et al.* [2010].

[13] In 2010, the Ocean Optic spectrometers of the initial version of the instrument were replaced by three new temperature controlled CTF60 spectrometers from OMT (Optische Messtechnik GmbH, Ulm, Germany) in order to increase the signal-to-noise ratio. They are Czerny-Turner type, using diffraction gratings with 2100 gr/mm, and cover the wavelength range of 286–423 nm with a spectral resolution of about 0.5 nm FWHM. In this wavelength range, several trace gases, e.g., NO_2, SO_2, BrO and O_3,have absorption bands and thus are retrieved by DOAS. A back-thinned Hamamatsu CCD Sensor with 2048 × 122 Pixels ist used in line binning mode, resulting in 2048 Pixels.

[14] A spectrum is taken every 8 seconds, but to reduce the measurement errors, usually 10 spectra are co-added, resulting in a temporal resolution of 80 seconds. As the speed of the aircraft is ∼250 m/s, this corresponds to a spatial resolution of 2 km or 20 km along the flight route.

[15] The first mission of the new DOAS system was in spring 2010 observing the plume of the Eyjafjallajökull volcano, see *Heue et al.* [2011].

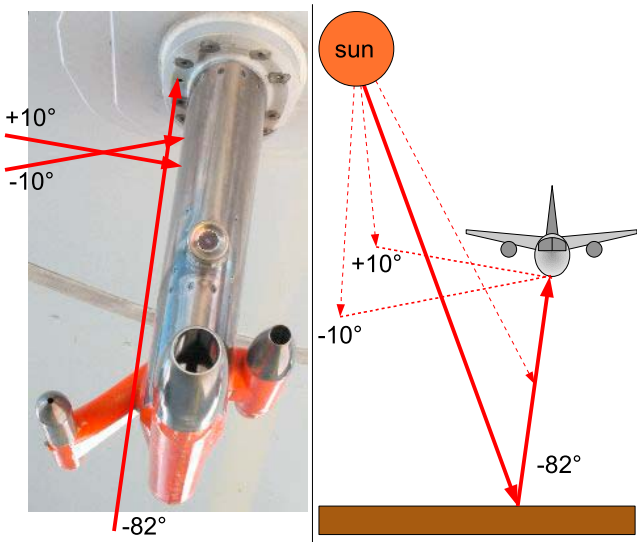

Figure 2. (left) Picture of the CARIBIC inlet pylon (∼35 cm tall), containing three tiny telescopes with two viewing directions close to the horizon (+10°, −10°) and a "nadir" direction (−82°). (right) Possible light paths from the sun to the telescope are sketched. The position of the inlet pylon itself is offset 8° anti-clockwise looking in flight-direction.

2.3. DOAS

[16] Differential Optical Absorption Spectroscopy (DOAS) is a spectroscopic analytical method widely used in atmospheric science for remote sensing of trace gases. It was introduced by *Platt et al.* [1979]. For detailed information about DOAS we refer to the recent compilation by *Platt and Stutz* [2008].

[17] DOAS is based on the Lambert-Beer-law:

$$I(\lambda) = I_0(\lambda) \cdot \exp\left(-\int \sigma(\lambda) \cdot c(l) \cdot \mathrm{d}l\right) = I_0(\lambda) \cdot \mathrm{e}^{-\sigma(\lambda) \cdot S} \quad (1)$$

It describes the reduction in the intensity I_0 of light when passing through a medium with absorption cross section $\sigma(\lambda)$ and number concentration c. The concentration integrated along the light path dl is called Slant Column Density (SCD), S:

$$S = \int c(l) \cdot \mathrm{d}l \quad (2)$$

For a mixture of gases, in this case the atmosphere, equation (1) becomes

$$I(\lambda) = I_0(\lambda) \cdot \exp\left(-\sum_i \int \sigma_i(\lambda) \cdot c_i(l) \cdot \mathrm{d}l\right) = I_0(\lambda) \cdot \exp\left(-\sum_i \sigma_i(\lambda) \cdot S_i\right) \quad (3)$$

[18] The cross sections of the relevant gases are taken from laboratory measurements. By measuring the intensities I_0 and I, the SCD of selected trace gases can be retrieved simultaneously using a least squares fit.

[19] However, only spectrum I is measured directly, whereas spectrum I_0 denotes the intensity of the solar light before entering the atmosphere, which can not be measured with the instrument. Therefore a "Fraunhofer reference spectrum" (FRS) measured above a 'pristine' area is used as a substitute for I_0. The retrieved value S_i then describes the difference between the absolute SCD of spectrum I and the absolute SCD of spectrum I_0. Thus it is called "differential Slant Column Density" (dSCD). If the spatial and temporal difference between the measure spectrum I and the reference spectrum I_0 is not too large, the light path through the stratosphere is nearly identical, by which the stratospheric contribution for the respective trace gas is removed automatically. Here, the FRS was taken at 07:10 UTC (90.3°E, 69.2°N) at a solar zenith angle (SZA) of 81.5°, five minutes before observing the maximum of the plume. For simplicity, in the following, "SCD" is used instead of "dSCD".

[20] Rayleigh and Mie scattering by molecules and aerosol particles influence the retrieval of the SCDs. This problem can be solved by adding an additional polynomial to the fit routine. The scattering processes have a broad-band structure and therefore are approximated by the polynomial, whereas the narrow-banded ("differential") absorption structures of the gases remain largely uninfluenced by the scattering polynomial. Inelastic scattering of light [*Grainger and Ring*, 1962] causes a filling-in of the Fraunhofer lines. In order to correct for this effect, a Ring spectrum [*Bussemer*, 1993] is calculated from the reference spectrum and included in the fit scenario.

[21] For the SO_2 retrieval, a wavelength range of 311.6–327.0 nm was taken, which is very similar to the one used for the GOME analysis (section 4.3). The cross-sections of the following trace gases were taken from literature and included in the DOAS fit: NO_2 [*Vandaele et al.*, 1996], BrO [*Wilmouth et al.*, 1999], HONO [*Stutz et al.*, 2000], SO_2 [*Bogumil et al.*, 2003], O_3 [*Voigt et al.*, 2001] as well as a Ring spectrum [*Bussemer*, 1993]. For the NO_2 retrieval, a wavelength range of 337.5–371 nm was taken, including a literature spectrum of the oxygen dimer O_4 [*Greenblatt et al.*, 1990]. Figure 3 shows the result of such a fit scenario for the case of a co-added spectrum, which was taken over the plume of Norilsk and evaluated with the program "WinDOAS" [*Fayt and van Roozendael*, 2001].

[22] Besides the retrieved SCD, a radiative transfer model and assumptions about the vertical distribution are used for the emission estimation. This is described in section 3.3.

3. Observations and Flux Calculation

3.1. Observations

[23] On Friday, 22 October 2010, the aircraft flew from Osaka to Frankfurt, taking a route far north which passed about 6 km south of Norilsk (Figure 4) at ~07:15 UTC, which corresponds to 15:15 local time (UTC+8) or 13:08 solar time (88.2°E).Taking into account that the viewing direction of the 'nadir' telescope is 8° to the right (in flight direction, cf. Figure 2), the closest distance to the stacks of Norilsk Nickel was roughly 5 km. The aircraft's altitude was 10.6 km above sea level.

[24] As the wind came from the north, the aircraft flew over the plume of Norilsk industries which could be clearly detected by the nadir instrument (Figure 4). Because there was little sunlight (the Solar Zenith Angle was around 81.5°), 10 spectra were co-added to increase the signal-to-noise-ratio, resulting in a maximum SCD of $6.2 \cdot 10^{17}$ molec/cm^2. This value was retrieved using a DOAS fit as described in section 2.3.

[25] In Figure 4, the retrieved NO_2 SCD is also shown with a clear peak at 07:15 UTC. However, this peak is only about 2% of the SO_2 peak. A second NO_2 peak is observed around 07:23 UTC. At that time, the aircraft flew over "Dudinka", the seaport of Norilsk Nickel.

3.2. Flux Calculation: Theory and Assumptions

[26] The idea behind the retrieval of the source strength of a species (here SO_2) by flux measurements is the continuity equation:

$$Q_{\mathrm{net}} = \oint_{\mathrm{surface}} \vec{J} \cdot \mathrm{d}\vec{A}_{\mathrm{area}} + \int_{\mathrm{volume}} \frac{\partial c}{\partial t} \cdot \mathrm{d}V_{\mathrm{vol}} \quad (4)$$

i.e., the net source strength Q_{net} inside a closed volume V_{vol} is the sum of the flux, J, through the surface A_{area} of the volume plus the change of the number concentration inside the volume. If sinks due to chemical reactions are involved, Q_{net} is the difference between the sources and the sinks.

[27] In the following, we describe our approach to determine the source strength Q of the MMC facilities at Norilsk. To get this value, the following assumptions are made (their discussion is contained in section 4.2):

[28] 1. $Q_{\mathrm{net}} = Q$, i.e., the Nickel Mine is the only source of the detected SO_2 and there are no sinks.

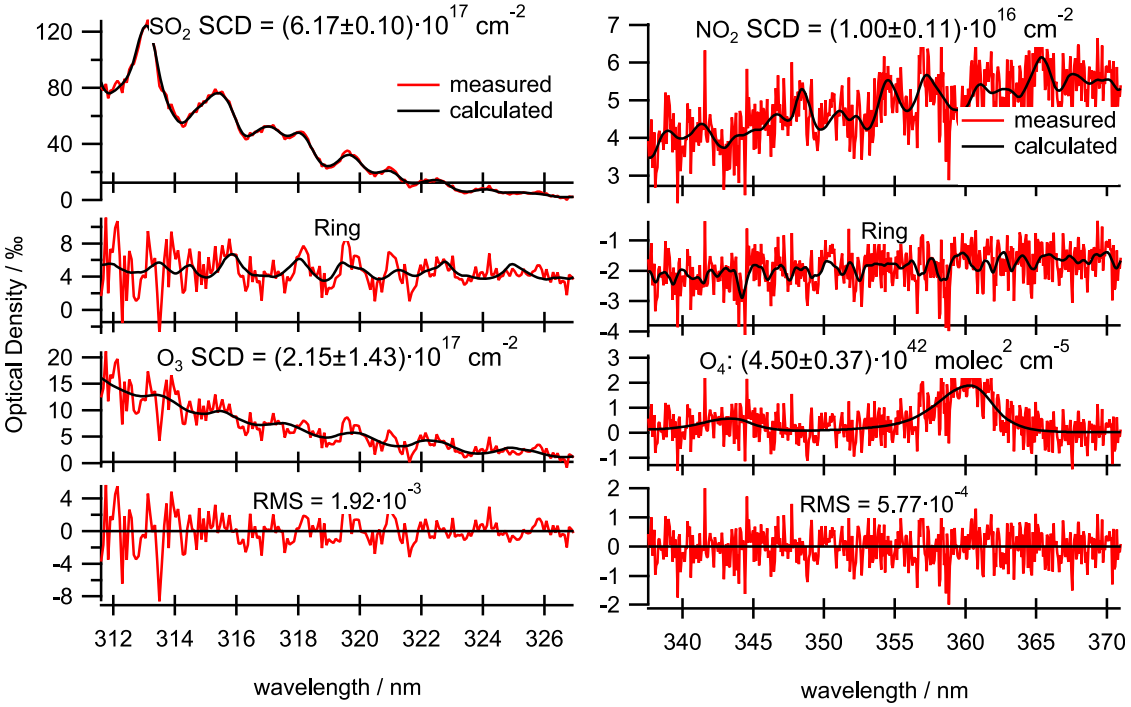

Figure 3. Example fit for a co-added spectrum (07:15:06–07:16:26 UTC on 22 Oct. 2010, cf. maximum value of the blue line in Figure 4). (left) Fitting window for SO_2 retrieval (311.6–327 nm). (right) Fitting window for NO_2 retrieval (337.5–371 nm).

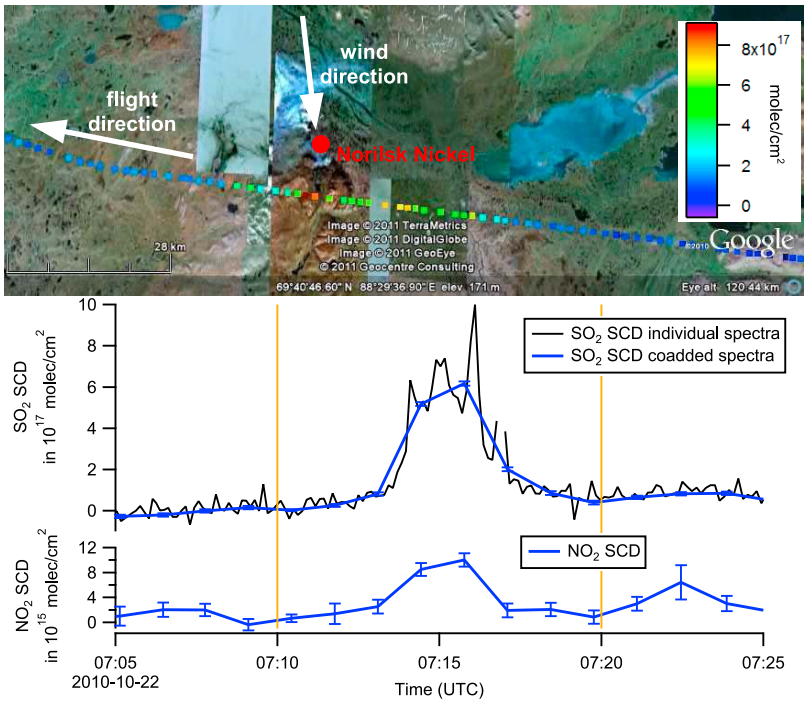

Figure 4. (top) Section of the flight route between 07:10 and 07:20 UTC on 22 Oct. 2010, color-coded with the SO_2 SCD (individual spectra). The red dot shows the position of industrial facilities of Norilsk Nickel. (bottom) Time series of SO_2 and NO_2. The black line corresponds to the dots in the top part. For reducing noise, co-added spectra were evaluated (blue lines).

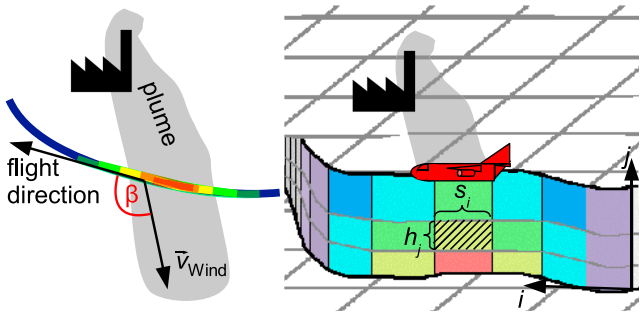

Figure 5. Flux calculation. (left) The angle β between the flight direction and the wind direction. (right) The discretization of the area under the flight route is depicted, showing a box of height h_j and length s_i as used in equation (7).

[29] 2. The amount of SO_2 inside the volume is constant; i.e., we assume steady state conditions. This simplifies equation (4) to

$$Q_{\text{net}} = \oint_{\text{surface}} \vec{J} \cdot \mathrm{d}\vec{A}_{\text{area}} \tag{5}$$

[30] 3. The flight route crosses over the complete plume. Then equation (5) can be written as

$$Q = \int \vec{J} \cdot \mathrm{d}\vec{A}_{\text{area}} = \int c \cdot \vec{v} \cdot \mathrm{d}\vec{A}_{\text{area}} \tag{6}$$

or in a discrete form with $\mathrm{d}\vec{A}_{\text{area}} = \vec{A}_{\text{area}i,j} = h_j \cdot s_i$ as

$$Q = \sum_i \left(s_i \cdot \sum_j h_j \cdot c_{i,j} \cdot v_{i,j} \cdot \sin\beta_{i,j} \right) \tag{7}$$

Here, s_i is the width and h_j is the height of a cell of the chosen grid box (hatched rectangle in Figure 5). $\beta_{i,j}$ is the angle between the flight route and the wind direction in grid cell i, j. The wind speed $v_{i,j}$ is obtained using a FLEXPART interpolation (Version 8.2) [*Stohl et al.*, 2005] based on 3 hourly 1° × 1° ECMWF data, see Figure 6. $c_{i,j}$ is the SO_2 concentration and is calculated based on the SCD (see following section).

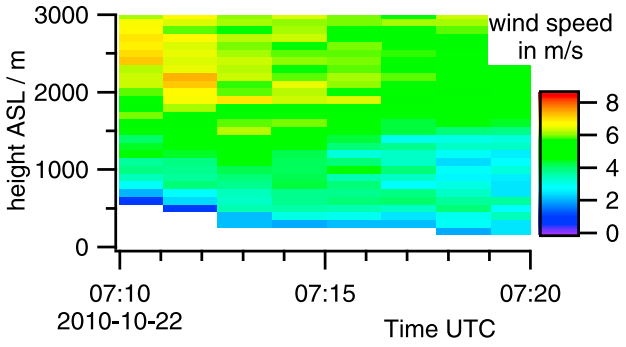

Figure 6. Wind speed below the flight trajectory based on ECMWF data. The time period of 10 minutes corresponds to a distance of about 140 km. The wind came approximately from the north.

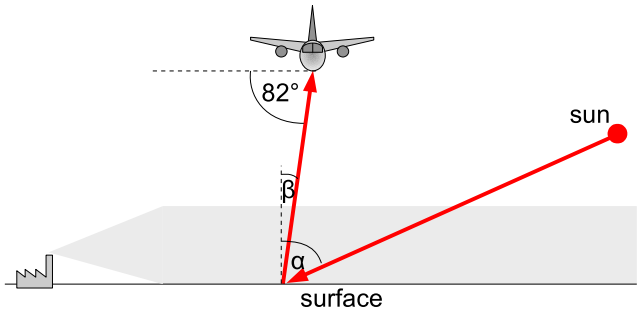

Figure 7. Geometric light path for direct sunlight. The light passes through the plume twice. In relation to the plume's height, the light path is stretched by a factor 1/cos α before and by 1/cos β after the reflection at the ground.

3.3. Retrieval of the Concentration Incorporating Radiative Transfer

3.3.1. Radiative Transfer, Vertical Column Density

[31] The SCD describes the concentration integrated along an average light path (equation (2)). A more useful quantity is the Vertical Column Density (VCD), which is defined as the concentration vertically integrated over the height:

$$V = \int \mathrm{d}h \cdot c(h) = \sum_j h_j \cdot c_j \tag{8}$$

The ratio between the SCD, S, and the VCD, V, is called "Air Mass Factor" (AMF): $A = S/V$. In the simplest case, the light passes through the plume twice – before and after having been reflected by the ground (see Figure 7). Then the geometric AMF can be used:

$$A = \frac{S}{V} = \frac{1}{\cos\alpha} + \frac{1}{\cos\beta} \tag{9}$$

With $\beta = 90^\circ - 82^\circ = 8^\circ$ for the nadir telescope and Solar Zenith Angle $\alpha = 81.5^\circ$ this results in $A = 7.78$.

[32] However, this would only be valid if no atmospheric scattering (cf. diffuse light) would appear. Especially for high SZA, scattering processes gain importance and the sensitivity in the lower altitudes decreases. To account for that, the AMF has to be calculated for several altitude boxes, the so-called Box-AMF, $A_j = S_j/V_j$. Thus, the SCD can be written as

$$S = \sum_j S_j = \sum_j A_j \cdot h_j \cdot c_j \tag{10}$$

[33] For the retrieval of the Box-AMF A_j, the radiative transfer model "McArtim" [*Deutschmann*, 2009] was used, which simulates photon pathways based on a Monte Carlo method. Therefore an SZA of 81.5°, a ground height of 0.2 km above sea level and an upper plume height of 1.5 km (cf. section 3.3.2) was taken. A standard profile for ozone and air pressure was included. A crucial value is the surface albedo. Here, 90% was used (assuming a snow covered surface, cf. section 4.2.2). The resulting Box-AMF are shown in Figure 8.

3.3.2. Relative Concentration Profile

[34] The result of the DOAS fit is an SCD. To get the concentrations for different heights, a relative concentration

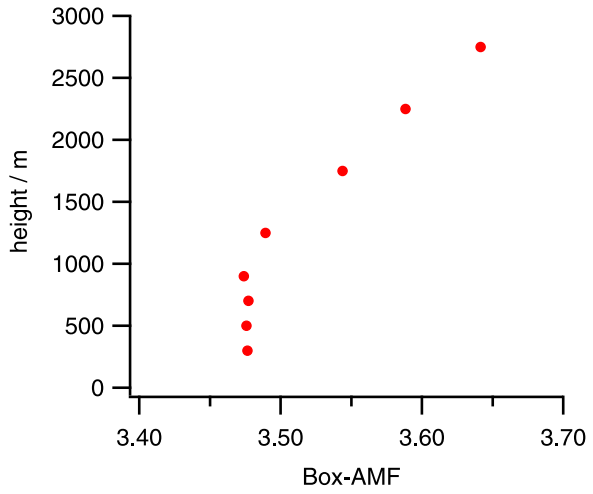

Figure 8. Vertical profile of the Box-AMF retrieved by the Monte-Carlo based Radiative Transfer Model "McArtim" for scenario 1 (cf. Table 1).

profile $c_R(h)$ (or c_{Rj} for the discrete case) has to be assumed, e.g., a box profile as shown in Figure 9b. Here, the concentration was assumed to be vertically constant within the boundary layer with an upper height of ~1.5 km. That value was estimated by regarding the ECMWF wind field (which increased significantly above 1.5 km) and the potential temperature from radio soundings. Because those soundings were taken ~400 km away from Norilsk, the value 1.5 km is only a rough estimate, cf. section 4.2.

[35] Using c_{Rj}, equation (10) can be written as

$$S = \sum_j A_j \cdot h_j \cdot c_{Rj} \cdot \left(\frac{c_j}{c_{Rj}}\right) \tag{11}$$

The assumption of a relative concentration profile means that the ratio (c_j/c_{Rj}) between the real concentration c_j and the relative concentration c_{Rj} shall be the same for each height h_j. Then this ratio can be factored out from the sum:

$$S = \left(\frac{c_j}{c_{Rj}}\right) \cdot \sum_j A_j \cdot h_j \cdot c_{Rj} \tag{12}$$

and the equation can be resolved for the desired concentration:

$$c_{i,j} = \frac{c_{Rj}}{\sum_j A_j \cdot h_j \cdot c_{Rj}} \cdot S_i \tag{13}$$

Here, the index i was added to indicate that the SCD, S_i, and, therefore, also the concentrations, $c_{i,j}$, horizontally change along the flight route, whereas the relative profile, c_{Rj}, was assumed to be constant in the relevant part.

3.3.3. Total AMF

[36] Although not explicitly needed for the flux calculation according to equations (7) and (13), the total AMF, $A = S/V$, can be calculated for a given (relative) conc. profile (cf. equations (8) and (10)):

$$A = \frac{S}{V} = \frac{\sum_j A_j \cdot h_j \cdot c_j}{\sum_j h_j \cdot c_j} = \frac{\sum_j A_j \cdot h_j \cdot c_{Rj}}{\sum_j h_j \cdot c_{Rj}} \tag{14}$$

The AMF values A are listed in the second column in Table 1.

4. Results, Discussion and Comparison With Other Data

4.1. Results

[37] Combining the measured SCD (Figure 4) with the assumed relative concentration (Figure 9b), the concentration profile, $c_{i,j}$, is calculated according to equation (13). It is depicted in Figure 9a in terms of a mixing ratio (for a pressure of 10^5 Pa). Multiplying the concentration by the wind speed $v_{i,j}$ (Figure 6) and considering the wind direction $\beta_{i,j}$ according to equation (7) leads to the flux pattern illustrated in Figure 9c. The desired total flux is the sum of all pixels, being $2.75 \cdot 10^{26}$ molecules per second. With a molar mass of 64.1 g for SO_2, this corresponds to 29.3 kg/s. Extrapolated to a whole year this leads to an integrated annual output of 0.92 Mt SO_2, assuming this single measurement to be representative, cf. discussion.

4.2. Assumptions and Accuracy

4.2.1. Flux Calculation

[38] In the following, the assumptions for the flux calculation made in section 3.2 are discussed.

[39] 1. $Q_{net} = Q$ The wind is coming from the north (Arctic Ocean, Kara Sea), passing about 600 km of Northern Siberia before it blows over Norilsk. In that area, the population density is very low and there are no big industrial activities. Hence Norilsk can be considered to be the only SO_2 source for the measured plume.

[40] To take sinks into account, the loss by oxidation of SO_2 has to be considered. The atmospheric lifetime of SO_2 is typically on the order of one day. The distance from the industrial plant to the flight track is between 5 and 10 km. With a wind speed in the range of 2 to 5 m/s this corresponds to a residence time between the emission and the detection of less than one hour. For an exponential decay $N(t) = N_0 \cdot e^{-t/\tau}$,

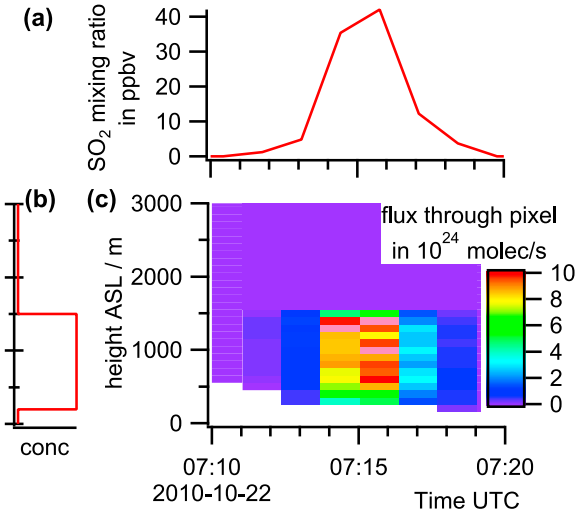

Figure 9. (a) Derived mixing ratio in the lowermost 1.5 km. (b) Assumed relative concentration profile: constant until 1.5 km altitude, zero above. (c) Flux pixel calculated from the SCD, relative concentration profile and wind data.

Table 1. Overview Over the Different Scenarios[a]

Scenario	Total AMF	Result (molec/s)	Result (Mt/year)	Rel. Diff.[b]	Notes
(1) 'standard'	3.46	2.75E+26	0.92	0%	
(2) decay of SO_2	3.46	2.87E+26	0.96	+4%	SO_2 lifetime: 1 day
(3) wind for 6:15	3.46	2.74E+26	0.92	−0.3%	
(4) raw wind data	3.41	3.25E+26	1.09	+18%	simplistic interpolation of ECMWF wind data
(5) other fitting window	3.99	3.34E+26	1.12	+22%	320–342 nm, McArtim simulation at 330 nm
(6) ground albedo: 0.6	2.37	4.03E+26	1.35	+47%	
(7) McArtim 325 nm	3.87	2.46E+26	0.83	−11%	
(8) aerosol extinction	2.19	4.34E+26	1.46	+58%	aerosol extinction coeff. 0.4/km
(9) geometric AMF	7.78	1.23E+26	0.41	−55%	no scattering, unrealistic
(10) plume height 2 km	3.40	3.07E+26	1.03	+12%	plume height 2 km instead of 1.5 km
(11) plume height 1 km	3.50	2.51E+26	0.84	−9%	plume height 1 km instead of 1.5 km
(12) plume height 0.6 km	3.42	2.15E+26	0.72	−22%	plume height 0.6 km instead of 1.5 km
(13) exp. conc. profile	3.46	2.73E+26	0.92	−0.6%	const. mixing ratio instead of const. concentration

[a]Scenario 1 is the 'standard' scenario. The other scenarios are based on scenario 1 but with certain differences.
[b]Relative difference compared to scenario 1.

this means that the amount of SO_2 has been reduced by ∼4% (for $t = 1$ h and $\tau = 24$ h). Taking this decay into account, the estimated source strength would slightly increase to $2.87 \cdot 10^{26}$ molec/s or 0.96 Mt/year (scenario 2 in Table 1).

[41] 2. The amount of SO_2 inside the volume remains constant, assuming a steady state situation. For this, first of all, the source strength has to be constant. For smaller industrial plants and for cities, this would probably not be the case due to diurnal, weekly and seasonal cycles. In our case this should be fulfilled, as smelting furnaces usually run 24 hours a day and 7 days per week. However, at least the extrapolation to the annual output has to be treated with caution.

[42] To ensure a steady state, also the wind has to be constant in the time interval of ∼1 hour between emission and detection. To get an estimate of the variability of the wind, the wind along the flight route was re-calculated for ≈6:15 UTC instead of ≈7:15 UTC. The difference of the wind speed between the two wind fields was ∼5%. A wind change in that time interval does not necessarily change the obtained result significantly, as only the wind up to the maximum plume height at the time of observation is used in the calculation of the flux. Indeed, the result of the flux calculation hardly changed when using the 6:15-wind-data (less than 1%, cf. scenario 3 in Table 1). The short term temporal variability of the wind (over seconds to minutes) is averaged out by the model, which can be regarded as a statistical error source. Therefore repeated measurements would help to reduce that problem. From a single measurement it is not possible to determine this error.

[43] Additionally it has to be mentioned, that the wind data based on ECMWF contain systematic errors as well. At least in the lower altitudes close to the ground, the values contain significant uncertainties due to small-scale convection which cannot be resolved in the model.

[44] Apart from the FLEXPART based interpolation, also ECMWF raw data were used, applying a linear interpolation in space and time for the relevant coordinates. With that, the result increased by 18% (see scenario 4 in Table 1), which can be explained by large errors due to the simplistic interpolation approach compared to the one used in the FLEXPART model.

[45] 3. The flight path of the aircraft crosses over the whole plume. As the aircraft's altitude is more than 10 km a.s.l. and the aircraft was flying straight across the plume, this assumption is fulfilled. This is confirmed by the fact that the plume was not detected in the $-10°$ looking channel. However, it has to be mentioned, that the plume could have been partly obscured by a cloud. But in that case the length of the light path would have changed due to changes in the scattering inside the cloud. This was not observed.

4.2.2. SCD, Radiative Transfer, Profile

[46] The statistical DOAS retrieval error in the time interval used for the flux calculation is on the order of 3%, which is negligible relative to the other uncertainties. However, the retrieved SCD shows some dependency on the wavelength range selected for the fit, and cross sensitivities, mainly to ozone, increase the uncertainties (cf. Table 1 scenario 5).

[47] The retrieval of the Box-AMF depends on several factors: A ground albedo of 0.9 (due to snow coverage) was used for the calculation in the 'standard' scenario (Table 1 scenario 1). Changing the albedo from 0.9 to 0.6 causes a decrease of the AMF from 3.46 to 2.37, as the fraction of light reflected from the surface decreases. This results in larger VCDs and concentrations and thus in an increase in the flux calculation of 47% to 1.35 Mt/year (Table 1 scenario 6).

[48] Changing the wavelength for the radiative transfer simulation from 315 nm to 325 nm leads to an AMF of 3.87 and a decrease of the flux calculation of 11%, giving 0.83 Mt/year (scenario 7). A strong influence is given by aerosol. In Scenario 8, an aerosol extinction coefficient of 0.4/km is assumed for the boundary layer (1.5 km) which leads to a much smaller AMF and therefore to a larger flux. Using the geometrical AMF $A = 7.78$ (equation (9)) results in 0.41 Mt/year (scenario 9). This has to be regarded as a lower (but unrealistic) limit for the radiative transfer, as it describes the unrealistic case, in which no light would have been scattered in the atmosphere.

[49] The vertical profile of the plume is a further uncertainty. First, it influences the calculation of the AMF. Secondly, it can be interpreted as a weighting function for the wind speed (equation (7) and Figure 9): In a high plume, the strong wind yields a strong contribution to the total flux, resulting in a higher flux estimation. In the case of our Norilsk observation, the sensitivity of the result with respect to the plume height was rather low. If the box height was not 1.5 km (like in the 'standard scenario') but 2 km, the result would increase by 12% to 1.03 Mt/year (scenario 10). For a height of 1 km (scenario 11), it would decrease by 9% to

0.84 Mt/year. Therefore it can be supposed that also the unknown real profile would lead to a similar result. However, in case of an upper plume height of 0.6 km, only 0.72 Mt/year would be calculated.

[50] The flux calculation according to equation (7) also allows the assumption of non-constant profiles. For a well-mixed boundary layer, a constant mixing ratio instead of a constant concentration is more convenient, leading to an exponential conc. profile (Barometric formula). Here, this difference is quite small (scenario 13), because the pressure decreases by only ~15% in the lowermost 1.5 km.

4.3. Comparison With GOME 1996–2002 Literature Value

[51] The Global Ozone Monitoring Experiment (GOME) is a spectrographic instrument aboard the European Remote Sensing Satellite (ERS-2), which was launched in 1995. GOME has a spectral range of 240–790 nm at a spectral resolution between 0.2 and 0.4 nm. The ERS-2 satellite has a near-polar sun-synchronous orbit at an altitude of 795 km with a local equator crossing time at 10:30 [*Burrows et al.*, 1999]. Within three days, a global ground coverage (at the equator) is obtained from the 960 km across-track swath.

[52] The recorded spectra are analyzed based on DOAS (section 2.3) to retrieve SCDs of several trace gases like O_3, SO_2, NO_2 and BrO. In *Khokhar et al.* [2008], the retrieval of the SO_2 output of several industries is described, amongst them the Norilsk Nickel Company and other smelters, using data from the years 1996–2002. For their SO_2 evaluation, a spectral range of about 312 nm to 327 nm was chosen. To convert the SCD into VCD, the Radiative Transfer Model Tracy-II [*Deutschmann*, 2007] was used, which is the predecessor of the McArtim model used in this study.

[53] The emission was estimated by integrating the SO_2 VCD over an area around the source and assuming an average atmospheric lifetime τ. A region around Norilsk (85–92°E, 68–72°N) was evaluated, considering Norilsk Nickel to be the only source accounting for SO_2 in that area (see section 4.2).

[54] The annual emission E_{annual} was calculated using the following equation:

$$E_{\text{annual}} = \frac{\int V \cdot \mathrm{d}A_{\text{area}}}{\tau} \cdot 365\,\text{days} \qquad (15)$$

V is the SO_2 Vertical Column Density, τ the atmospheric lifetime of SO_2. This lifetime is highly variable [*Stevenson et al.*, 2003], as it depends on various parameters like temperature, solar radiative flux, precipitation, humidity and wind. Also the presence of clouds and the altitude of the SO_2 plume play an important role [*Graf et al.*, 1997; *Khokhar*, 2006]. Typically reported values for τ are between 0.6 and 2.4 days for boundary layer anthropogenic emissions [*Khokhar et al.*, 2008; *Atkinson et al.*, 2007; *Brasseur et al.*, 1999; *von Glasow et al.*, 2002].

[55] For their calculation, *Khokhar et al.* [2008] chose a lifetime of one day. They obtained an emission estimate for Norilsk of 1.685 ± 0.3 Mt SO_2 per year in 1996–2002. For an SO_2 lifetime of 2 days, half the emission would be calculated.

4.4. Comparison With OMI SO_2 for 2010-10-22

[56] The Ozone Monitoring Instrument (OMI) is a spectrographic instrument aboard the "Aura" satellite launched in July 2004 [*Levelt et al.*, 2006]. It has a spectral range from 264 nm to 504 nm with a spectral resolution of about 0.5 nm. In contrast to GOME, no scanning mirror is used to obtain spatial information perpendicular to the flight track, but rather, it uses a two-dimensional CCD detector. OMI has a swath width of 2600 km. As OMI performs 14 orbits a day, a daily global coverage can be provided. The spatial resolution is 13 km by 24 km (48 km for the UV-1 channel) at nadir position, becoming broader toward the outer swath-angle of 57°.

[57] The Sulfur Dioxide Group evaluates and validates SO_2 column densities [e.g., *Carn and Lopez*, 2011]. Due to the large solar angles in Siberia during October, the lack of sufficient sunlight makes satellite SO_2 retrievals difficult and imprecise. Nevertheless, for 22 October 2010 data is available from an OMI overpass at 05:38 UTC, about 1.5 hours prior to CARIBIC's overpass time (see Figure 10).

[58] We used a similar approach as mentioned above (section 4.3) to estimate the source strength for that particular day. Therefore, the SO_2 emitted within 24 hours before the overpass of OMI was assumed to be within a circle of 111 km radius (1° of latitude) around the estimated center of the plume. To remove the background signal, an offset was subtracted in a way that the average of the pixel's values outside the circle vanished (Figure 10). Summing up all the values inside the circle equals to about $1.7 \cdot 10^{31}$ molecules. This value depends on the chosen radius. Taking too small a radius leads to an underestimated value because the complete plume is not inside, whereas too large a radius contains too much noise from the background. Forward trajectories from HYSPLIT (R. Draxler and G. D. Rolph, HYSPLIT (HYbrid Single-Particle Lagrangian Integrated Trajectory) model, 2011, http://ready.arl.noaa.gov/HYSPLIT.php) indicate that it might be reasonable to vary the circle between 80 and 160 km (Figure 10). This results in values from $1.5 \cdot 10^{31}$ to $2.3 \cdot 10^{31}$ molecules. Using an SO_2 lifetime of one day leads to an SO_2 output of $\approx 2 \cdot 10^{26}$ molec/s ($1.7 \cdot 10^{26}$ to $2.7 \cdot 10^{26}$ molec/s respectively), corresponding to an annual output of 0.7 Megatons (0.6 to 0.9 Mt), which is in agreement with the results from the CARIBIC measurements, considering the uncertainties of both approaches. Again, the SO_2 lifetime is a critical parameter, cf. section 4.3.

4.5. Miscellaneous Literature Values

[59] According to the EDGAR database, the production of metals in the Russian Federation caused about 2.5 Mt of SO_2 emission in the year 2005. This database also contains emission maps, one of them called "Industry combustion and process emissions". Summing up the SO_2 emission in that map in a grid box around Norilsk (87.7–88.4°E, 68.9–69.6°N) leads to annual emission estimates between 0.63 Mt and 0.73 Mt in the years 1995 to 2005.

[60] In the report "The World's Worst Polluted Places" of the *Blacksmith Instititute* [2007], an annual SO_2 emission of 2 Mt is reported for the Norilsk emissions. Also according to *Carn et al.* [2004], the emission is "variously reported as being on the order of 2–3 Megatons (Mt) per year". According to the report "Commitment to Environmental Protection" of the Norilsk Nickel Company [*Norilsk Nickel*, 2009], the SO_2 emission of the "Group's Operations in the Russian Federation" is about 2.1 Mt for the years 2007–2009. However, it is not mentioned, which fraction of that amount is related to the "Taimyr Peninsula" (Norilsk). In a

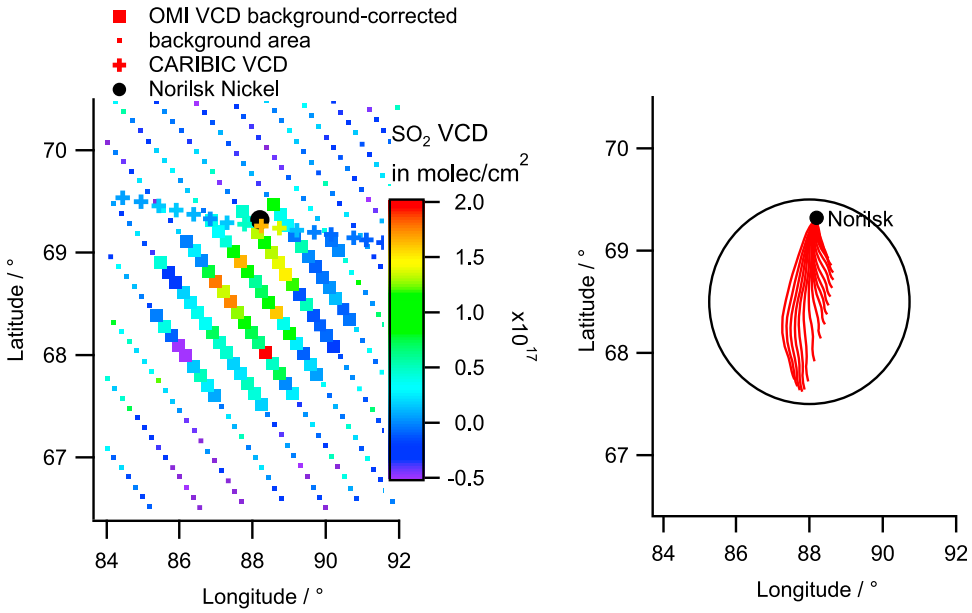

Figure 10. (left) OMI SO_2 measurement (squares) compared to CARIBIC (crosses). The big squares are used for the calculation of the amount of SO_2 in the plume. (right) One-day forward trajectories created through the HYSPLIT web interface (http://ready.arl.noaa.gov/HYSPLIT.php), starting at Norilsk Nickel between 21 Oct. 2010 06:00 and 22 Oct. 2010 05:00, ending at 22 Oct. 2010 06:00. The black circle (radius 111 km) refers to the thick squares on the left side.

recommendation of the Norwegian "Council on Ethics" [*Leder et al.*, 2009], also around 2 Mt are mentioned (1.94 Mt for 2006 and 2007). The same report mentions a plan of Norilsk Nickel to reduce the SO_2 emission levels by 70% by 2010, but it also says that "SO_2 emission levels are nearly unchanged" and "The company's plans to significantly reduce emissions have so far not been implemented."

4.6. Comparison of NO_2 With OMI

[61] As depicted in Figure 4, also NO_2 was observed by the CARIBIC DOAS instrument. The same is true for the OMI measurement that took place at 05:38 UTC (cf. 4.4). For comparison, the VCD are plotted in Figure 11. In the OMI retrieval, the total VCD is separated into a stratospheric and a tropospheric part (which is depicted here). For CARIBIC, a reference spectrum taken shortly before 07:10 UTC is used, so the stratospheric part is removed automatically. For the conversion from SCD to VCD, a box profile of 1.5 km height was assumed like in the case of SO_2 (Figure 9b). The VCD depends on the assumed surface reflectance: For an albedo of 0.9, the maximum NO_2 VCD of CARIBIC is $2.31 \cdot 10^{15}$ molec/cm^2; for an albedo of 0.6, this value increases by 35% to $3.13 \cdot 10^{15}$ molec/cm^2. For the OMI data, a surface reflectance database is used with a snow albedo of 0.6. Using an albedo of 0.6, the CARIBIC and OMI results compare reasonably well, considering several differences between the two measurements. As already discussed for SO_2, there is a time difference between OMI and CARIBIC of ~1.5 hours and the spatial resolution of the two instruments is vastly different.

[62] We did not perform an emission estimate for NO_2 based on the OMI data like in section 4.3 and 4.4, because there is no 'constant lifetime' of NO_2 (cf. equation (15)). A flux calculation based on the CARIBIC data and equation (7) results in $3.7 \cdot 10^{24}$ molec/s (albedo 0.9) or $5.0 \cdot 10^{24}$ molec/s (albedo 0.6). This value does not represent the real amount of NO_2 emissions of Norilsk Nickel, as chemical reactions take place between emission and observation. However, the NO_2 emission probably

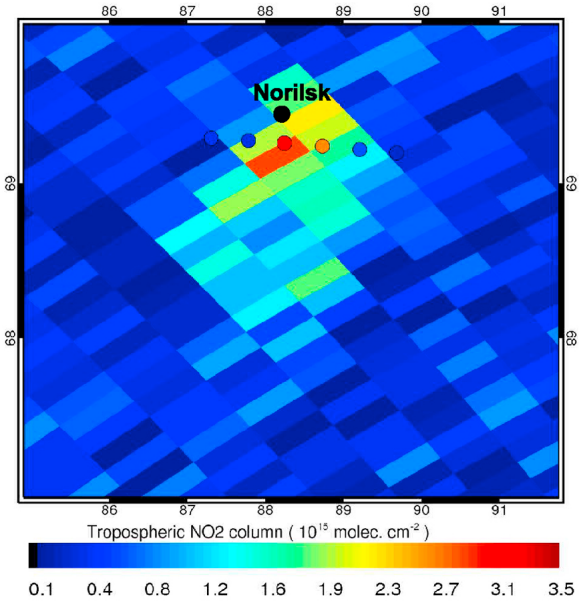

Figure 11. NO_2 VCD of OMI (rectangles, 05:38 UTC) and CARIBIC (circles, 07:10–07:20 UTC, assumed surface albedo: 0.6).

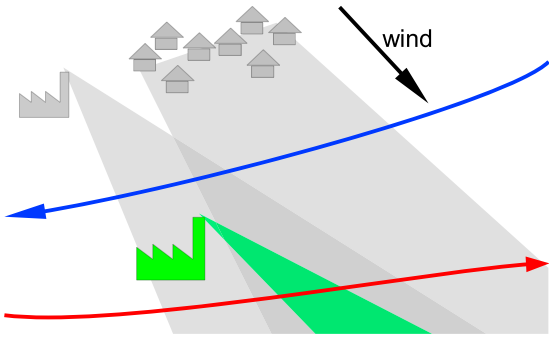

Figure 12. The flux under the red flight route contains the plume of several sources. To retrieve the output of a single source (green) the background (gray) can be corrected by subtracting the flux under the blue flight route.

represents 80% or more of the total NO_x emission, which can be estimated from the Leighton ratio [*Leighton*, 1961]:

$$L_{\text{Leighton}} := \frac{[\text{NO}]}{[\text{NO}_2]} = \frac{J_{\text{NO}_2}}{k \cdot [\text{O}_3]} \tag{16}$$

For a photolysis frequency $J_{NO_2} = 1.5 \cdot 10^{-3}\text{s}^{-1}$, a reaction constant $k = 1 \cdot 10^{-14}$ cm^{3}s^{-1} (see *Atkinson et al.* [2004], reaction between NO and O_3 for 265 K) and a ozone concentration of $5.4 \cdot 10^{11}$ cm^{-3} (20 ppb) it calculates to $L_{\text{Leighton}} \approx 0.2$. The value for the photolysis frequency is a rough estimate for clear viewing conditions [cf. *Koepke et al.*, 2010], the actual one might be lower, which would lead to an even lower L_{Leighton}.

5. Conclusions

[63] Based on the measurements of the CARIBIC DOAS instrument on 22 October 2010, the instantaneous SO_2 emissions of Norilsk Nickel were estimated to be $3 \cdot 10^{26}$ molec/s or 30 kg/s. For this estimate, ECMWF based wind data was used and it was assumed that the SO_2 plume was evenly distributed throughout the lowermost 1.5 km of the atmosphere. A quantitative error estimation cannot be given. The uncertainties in the wind field, the ground albedo and the AMF are supposed to be the main limiting factors. An extrapolation to an entire year leads to an SO_2 output of 1 Mt/year.

[64] The comparison with OMI satellite data for the same day shows a reasonably good agreement when using an SO_2 lifetime of one day. Compared to the results of *Khokhar et al.* [2008] for GOME measurements from 1996–2002, the CARIBIC estimate is roughly 50% lower. From our single measurement it is not possible to determine whether this difference indicates a decreasing trend of Norilsk's emissions or whether the measurement took place during a time of lower industrial activity – for this purpose further flights on this route are desirable. While the SO_2 lifetime τ is crucial for the approach used for the satellite data (the calculated flux is inversely proportional to τ, cf. equation (15)), it is of minor importance for flux measurements as long as the transport time between emission and detection is small in relation to the lifetime (cf. scenario 2).

[65] This study shows that airborne flux estimations are possible using DOAS onboard passenger aircraft. Such instruments are low-maintenance, because they contain no moving parts and need no calibration. They are small and low-weight and have a low power consumption. Furthermore, DOAS instruments (looking in flight direction) can serve as airborne early detection systems of SO_2 as indicator for volcanic plumes, as recently shown by *Vogel et al.* [2011]. Thus, DOAS instruments might be considered to be installed in commercial aircraft, offering repeated measurements of sources. Combining those results would allow for determining and decreasing the errors which are mainly caused by clouds and changes of the wind.

[66] By establishing a network of airborne DOAS instruments it would also be possible to measure the emission of individual (smaller) sources (see Figure 12). By subtracting the flux under one flight route from the flux under another flight route, it is possible to distinguish the emission of several sources from one another. If the temporal difference between the flight routes are small enough, this approach is feasible also for sources with a diurnal cycle like cities.

[67] **Acknowledgments.** The authors thank Lufthansa Airlines and Lufthansa Technik for their commitment and support, especially Andreas Waibel and Thomas Dauer. We would also like to thank Angela Baker and all members of the CARIBIC team. Further thanks go to the MPI-C satellite group, especially Christoph Hörmann and Steffen Dörner for the support concerning the wind data, which were kindly provided by ECMWF (http://www.ecmwf.int). The DOAS system was built and operated by the Institut für Umweltphysik of the Universität Heidelberg. The development and operation of the CARIBIC system has been financially supported by the German Ministry of Education and Science (AFO 2000), by the European Commission's DGXII Environment RTD 4th, 5th and 6th Framework programs, by the Max Planck Society and Frankfurt Airport. Data are available upon request; please visit http://www.caribic-atmospheric.com/ for more information. The service charges for this publication have been covered by the Max Planck Society.

References

Atkinson, R., D. L. Baulch, R. A. Cox, J. N. Crowley, R. F. Hampson, R. G. Hynes, M. E. Jenkin, M. J. Rossi, and J. Troe (2004), Evaluated kinetic and photochemical data for atmospheric chemistry: Volume I—Gas phase reactions of O_x, HO_x, NO_x and SO_x species, *Atmos. Chem. Phys.*, *4*(6), 1461–1738, doi:10.5194/acp-4-1461-2004.

Atkinson, R., D. L. Baulch, R. A. Cox, J. N. Crowley, R. F. Hampson, R. G. Hynes, M. E. Jenkin, M. J. Rossi, and J. Troe (2007), Evaluated kinetic and photochemical data for atmospheric chemistry: Volume III—Gas phase reactions of inorganic halogens, *Atmos. Chem. Phys.*, *7*(4), 981–1191, doi:10.5194/acp-7-981-2007.

Blacksmith Institute (2007), *The World's Worst Polluted Places—The Top Ten of The Dirty Thirty*, New York.

Bogumil, K., et al. (2003), Measurements of molecular absorption spectra with the SCIAMACHY pre-flight model: Instrument characterization and reference data for atmospheric remote-sensing in the 230–2380 nm region, *J. Photochem. Photobiol. A*, *157*(2–3), 167–184, doi:10.1016/S1010-6030(03)00062-5.

Brasseur, G., J. J. Orlando, and G. S. Tyndall (Eds.) (1999), *Atmospheric Chemistry and Global Change*, 654 pp., Oxford Univ. Press, New York.

Brenninkmeijer, C. A. M., et al. (2007), Civil aircraft for the regular investigation of the atmosphere based on an instrumented container: The new CARIBIC system, *Atmos. Chem. Phys.*, *7*(18), 4953–4976, doi:10.5194/acp-7-4953-2007.

Burrows, J. P., et al. (1999), The Global Ozone Monitoring Experiment (GOME): Mission concept and first scientific results, *J. Atmos. Sci.*, *56*(2), 151–175, doi:10.1175/1520-0469(1999)056<0151:TGOMEG>2.0.CO;2.

Bussemer, M. (1993), Der Ring-Effekt: Ursachen und Einfluß auf die spektroskopische Messung stratosphärischer Spurenstoffe, diploma thesis, Inst. für Umweltphys., Univ. Heidelberg, Heidelberg, Germany.

Carn, S. A., and T. M. Lopez (2011), Opportunistic validation of sulfur dioxide in the Sarychev Peak volcanic eruption cloud, *Atmos. Meas. Tech.*, *4*(9), 1705–1712, doi:10.5194/amt-4-1705-2011.

Carn, S. A., A. J. Krueger, N. A. Krotkov, and M. A. Gray (2004), Fire at Iraqi sulfur plant emits SO_2 clouds detected by Earth probe TOMS, *Geophys. Res. Lett.*, *31*, L19105, doi:10.1029/2004GL020719.

Chin, M., and D. J. Jacob (1996), Anthropogenic and natural contributions to tropospheric sulfate: A global model analysis, *J. Geophys. Res.*, *101* (D13), 18,691–18,699, doi:10.1029/96JD01222.

Crutzen, P. (2006), Albedo enhancement by stratospheric sulfur injections: A contribution to resolve a policy dilemma?, *Clim. Change*, *77*, 211–220, doi:10.1007/s10584-006-9101-y.

Deutschmann, T. W. (2007), *TRACY-II Manual 0.85*, Inst. für Umweltphys., Univ. Heidelberg, Heidelberg, Germany.

Deutschmann, T. (2009), Atmospheric radiative transfer modelling with Monte Carlo methods, diploma thesis, Instit. für Umweltphys., Univ. Heidelberg, Heidelberg, Germany.

Dix, B. (2007), Spectroscopic measurements of atmospheric trace gases on long-distance flights, Ph.D. thesis, Instit. für Umweltphys., Univ. Heidelberg, Heidelberg, Germany.

Dix, B., C. A. M. Brenninkmeijer, U. Frieß, T. Wagner, and U. Platt (2009), Airborne multi-axis DOAS measurements of atmospheric trace gases on CARIBIC long-distance flights, *Atmos. Meas. Tech.*, *2*(2), 639–652, doi:10.5194/amt-2-639-2009.

Environment Australia (1999), Emission estimation technique manual for nickel concentrating, smelting and refining, Natl. Pollut. Inventory, Everton Park, Queensland, Australia.

Fayt, C., and M. van Roozendael (2001), WinDOAS 2.1 software user manual, Belg. Inst. for Space Aeron., Brussels.

Galle, B., M. Johansson, C. Rivera, Y. Zhang, M. Kihlman, C. Kern, T. Lehmann, U. Platt, S. Arellano, and S. Hidalgo (2010), Network for Observation of Volcanic and Atmospheric Change (NOVAC)—A global network for volcanic gas monitoring: Network layout and instrument description, *J. Geophys. Res.*, *115*, D05304, doi:10.1029/2009JD011823.

Graf, H.-F., J. Feichter, and B. Langmann (1997), Volcanic sulfur emissions: Estimates of source strength and its contribution to the global sulfate distribution, *J. Geophys. Res.*, *102*(D9), 10,727–10,738, doi:10.1029/96JD03265.

Grainger, J. F., and J. Ring (1962), Anomalous Fraunhofer line profiles, *Nature*, *193*(4817), 762, doi:10.1038/193762a0.

Greenblatt, G. D., J. J. Orlando, J. B. Burkholder, and A. R. Ravishankara (1990), Absorption measurements of oxygen between 330 and 1140 nm, *J. Geophys. Res.*, *95*(D11), 18,577–18,582, doi:10.1029/JD095iD11p18577.

Heue, K.-P., C. A. M. Brenninkmeijer, T. Wagner, K. Mies, B. Dix, U. Frieß, B. G. Martinsson, F. Slemr, and P. F. J. van Velthoven (2010), Observations of the 2008 Kasatochi volcanic SO_2 plume by CARIBIC aircraft DOAS and the GOME-2 satellite, *Atmos. Chem. Phys.*, *10*(10), 4699–4713, doi:10.5194/acp-10-4699-2010.

Heue, K.-P., et al. (2011), SO_2 and BrO observation in the plume of the Eyjafjallajökull volcano 2010: CARIBIC and GOME-2 retrievals, *Atmos. Chem. Phys.*, *11*(6), 2973–2989, doi:10.5194/acp-11-2973-2011.

Khokhar, M. F. A. (2006), Retrieval and interpretation of tropospheric SO_2 from UV-VIS satellite instruments, Ph.D. thesis, Univ. Leipzig, Leipzig, Germany.

Khokhar, M. F., U. Platt, and T. Wagner (2008), Temporal trends of anthropogenic SO_2 emitted by non-ferrous metal smelters in Peru and Russia estimated from satellite observations, *Atmos. Chem. Phys. Discuss.*, *8* (5), 17,393–17,422, doi:10.5194/acpd-8-17393-2008.

Koepke, P., M. Garhammer, M. Hess, and E.-P. Roeth (2010), NO_2 photolysis frequencies in street canyons, *Atmos. Chem. Phys.*, *10*(15), 7457–7466, doi:10.5194/acp-10-7457-2010.

Leder, G. N., A. Follesdal, A. L. Gade, O. Mestad, and B. Ostbo (2009), Recommendation of February 16, 2009, on the exclusion of the company Norilsk Nickel, Norw. Counc. on Ethics, Oslo.

Leighton, P. A. (1961), *Photochemistry of Air Pollution*, *Phys. Chem.*, vol. 9, 300 pp., Academic, New York.

Levelt, P., G. van den Oord, M. Dobber, A. Malkki, H. Visser, J. de Vries, P. Stammes, J. Lundell, and H. Saari (2006), The ozone monitoring instrument, *IEEE Trans. Geosci. Remote Sens.*, *44*(5), 1093–1101, doi:10.1109/TGRS.2006.872333.

Martinsson, B. G., C. A. M. Brenninkmeijer, S. A. Carn, M. Hermann, K.-P. Heue, P. F. J. van Velthoven, and A. Zahn (2009), Influence of the 2008 Kasatochi volcanic eruption on sulfurous and carbonaceous aerosol constituents in the lower stratosphere, *Geophys. Res. Lett.*, *36*, L12813, doi:10.1029/2009GL038735.

Melamed, M. L., S. Solomon, J. S. Daniel, A. O. Langford, R. W. Portmann, T. B. Ryerson, D. K. Nicks Jr., and S. A. McKeen (2003), Measuring reactive nitrogen emissions from point sources using visible spectroscopy from aircraft, *J. Environ. Monit.*, *5*, 29–34, doi:10.1039/B204220G.

Norilsk Nickel (2009), Commitment to environmental protection; MMC Norilsk Nickel annual report 2009, chap. 8, pp. 107–115, Moscow. [Available at http://www.nornik.ru/en/investor/report/annual/year2009/.]

Platt, U., and J. Stutz (2008), *Differential Optical Absorption Spectroscopy*, *Phys. Earth Space Environ.*, vol. 15, 597 pp., Springer, Berlin.

Platt, U., D. Perner, and H. W. Pätz (1979), Simultaneous measurement of atmospheric CH_2O, O_3, and NO_2 by differential optical absorption, *J. Geophys. Res.*, *84*(C10), 6329–6335, doi:10.1029/JC084iC10p06329.

Stevenson, D. S., C. E. Johnson, E. J. Highwood, V. Gauci, W. J. Collins, and R. G. Derwent (2003), Atmospheric impact of the 1783-1784 Laki eruption: Part I Chemistry modelling, *Atmos. Chem. Phys.*, *3*(3), 487–507, doi:10.5194/acp-3-487-2003.

Stohl, A., C. Forster, A. Frank, P. Seibert, and G. Wotawa (2005), The Lagrangian particle dispersion model FLEXPART version 6.2, *Atmos. Chem. Phys.*, *5*(9), 2461–2474, doi:10.5194/acp-5-2461-2005.

Stutz, J., E. S. Kim, U. Platt, P. Bruno, C. Perrino, and A. Febo (2000), UV-visible absorption cross sections of nitrous acid, *J. Geophys. Res.*, *105* (D11), 14,585–14,592, doi:10.1029/2000JD900003.

Trainer, M., B. A. Ridley, M. P. Buhr, G. Kok, J. Walega, G. Hübler, D. D. Parrish, and F. C. Fehsenfeld (1995), Regional ozone and urban plumes in the southeastern United States: Birmingham, a case study, *J. Geophys. Res.*, *100*(D9), 18,823–18,834, doi:10.1029/95JD01641.

Vandaele, A. C., C. Hermans, P. C. Simon, M. Roozendael, J. M. Guilmot, M. Carleer, and R. Colin (1996), Fourier transform measurement of NO_2 absorption cross-section in the visible range at room temperature, *J. Atmos. Chem.*, *25*, 289–305, doi:10.1007/BF00053797.

Vogel, L., et al. (2011), Early in-flight detection of SO_2 via differential optical absorption spectroscopy: A feasible aviation safety measure to prevent potential encounters with volcanic plumes, *Atmos. Meas. Tech.*, *4*(9), 1785–1804, doi:10.5194/amt-4-1785-2011.

Voigt, S., J. Orphal, K. Bogumil, and J. P. Burrows (2001), The temperature dependence (203-293 K) of the absorption cross sections of O_3 in the 230–850 nm region measured by Fourier-transform spectroscopy, *J. Photochem. Photobiol. A*, *143*(1), 1–9, doi:10.1016/S1010-6030(01)00480-4.

von Glasow, R., R. Sander, A. Bott, and P. J. Crutzen (2002), Modeling halogen chemistry in the marine boundary layer: 2. Interactions with sulfur and the cloud-covered MBL, *J. Geophys. Res.*, *107*(D17), 4323, doi:10.1029/2001JD000943.

Wang, P., A. Richter, M. Bruns, J. P. Burrows, R. Scheele, W. Junkermann, K.-P. Heue, T. Wagner, U. Platt, and I. Pundt (2006), Airborne multi-axis DOAS measurements of tropospheric SO_2 plumes in the Po-valley, Italy, *Atmos. Chem. Phys.*, *6*(2), 329–338, doi:10.5194/acp-6-329-2006.

White, W. H., J. A. Anderson, D. L. Blumenthal, R. B. Husar, N. V. Gillani, J. D. Husar, and W. E. Wilson Jr. (1976), Formation and transport of secondary air pollutants: Ozone and aerosols in the St. Louis urban plume, *Science*, *194*(4261), 187–189.

Wilmouth, D. M., T. F. Hanisco, N. M. Donahue, and J. G. Anderson (1999), Fourier transform ultraviolet spectroscopy of the $A\ ^2\Pi_{3/2} \leftarrow X\ ^2\Pi_{3/2}$ transition of BrO, *J. Phys. Chem. A*, *103*(45), 8935–8945, doi:10.1021/jp991651o.